CrystEngComm

Accepted Manuscript

ROYAL SOCIETY OF CHEMISTRY

www.rsc.org/crystengcomm

Structural, Spectroscopic and Theoretical Studies of A Vapochromic Platinum(II) Terpyridyl Complex

Rui Zhang,[1] Zhenning Liang,[1] Ali Han,[2] Haotian Wu,[2] Pingwu Du,*[2] Wenzhen Lai,*[1] and Rui Cao*[1,3]

[1]*Department of Chemistry & Beijing Key Laboratory of Opto-electronic Functional Materials and Micro-nano Devices, Renmin University of China, Beijing, 100872, China;* [2]*CAS Key Laboratory of Materials for Energy Conversion & Department of Materials Science & Engineering, University of Science and Technology of China (USTC), Hefei, Anhui, 230026, China;* [3]*Department of Chemistry and Chemical Engineering, Beijing University of Technology, Beijing, 100124, China.*

*To whom correspondence should be addressed. E-mail: dupingwu@ustc.edu.cn, wenzhenlai@ruc.edu.cn, ruicao@ruc.edu.cn

Abstract: The vapochromism of the platinum(II) terpyridyl complex [Pt(tpy)Cl](PF$_6$) (**1**, tpy = 2,2':6',2"-terpyridine) was investigated. Complex **1** was found to exist in two forms. The yellow form of **1** turned to red by exposing the solid to either vapor or solution of acetonitrile, accompanying with changes in luminescent spectroscopy. This process could be reversed upon the loss of acetonitrile. Complex **1** was also demonstrated to show

aggregation in diethyl ether−acetonitrile system through Pt···Pt and terpyridyl π−π interactions to afford the red form of **1**. Crystals of the red and yellow forms of **1** were analyzed. The red form of **1** crystallizes in orthorhombic space group *Pnma* with a co-crystallized acetonitrile solvent molecule and thus is defined as **1**-MeCN, while the yellow form is found to have the previously reported non-solvated crystal structure of **1**. In **1**-MeCN, the square planar $[Pt(tpy)Cl]^+$ monocations stack to give an extended chain-like array of Pt atoms with a short Pt···Pt distance at 3.362 Å, while in **1**, there are two alternating Pt···Pt distances (4.032 and 3.340 Å). Time-dependent density functional theory (TDDFT) calculations demonstrated that Pt···Pt and terpyridyl π−π interactions play important roles in electronic absorption features of the $[Pt(tpy)Cl]^+$ system. Compared to dimers, the stack of three molecules of **1** with a short Pt···Pt distance considerably lowers the transition energy of metal-metal-to-ligand charge transfer (MMLCT), which causes a dramatic red shift in UV-vis spectroscopy.

Introduction

Design and development of stable chemical sensor materials that exhibit pronounced and reversible changes of physical and/or photophysical properties have attracted increasing attention because of their potential applications in sensing.[1-11] Recently, materials that show selective and tunable changes in electronic absorption and/or emission spectroscopy in the visible light region upon exposure to volatile organic compounds (VOCs) are of particular interest.[12-19] The VOC-induced responses usually originate from either a change in the molecular structure[20,21] (i.e. the coordination of

metal centers) or in the molecular packing that alters metal−metal distances and π−π interactions.[22-26]

Photofunctional transition metal complexes with d^6, d^8 and d^{10} electronic configurations have been demonstrated to be very valuable in a variety of photonic applications, including luminescent sensors, photocatalysis and photoelectrochemistry, due to their fascinating photophysical characters.[1,5,10,17,20,27] For example, a range of transition metal complexes of ruthenium(II),[28,29] iridium(III),[30] palladium(II),[31] platinum(II),[32-38] copper(I),[39] gold(I),[40-47] and zinc(II)[13,48] have been synthesized and found to exhibit intriguing luminescence properties, and many of them have been evaluated as vapochromic and/or vapoluminescent materials with practical applications. Among them, Pt(II) systems have been extensively studied owing to not only their rich spectroscopic features but also the ease to perturb and control their features by tuning the microenvironment of the Pt(II) center.[1,22]

Four-coordinate square-planar Pt(II) polypyridyl complexes have a strong tendency to form highly ordered extended linear chains or oligomeric structures in the solid state through the metal−metal interaction and the π−π interaction of polypyridyl ligands.[1,22,49-51] The relatively strong Pt−Pt interactions can significantly lower the metal-to-ligand charge transfer (MLCT) energy, and thus enrich their spectroscopic and luminescent properties.[1,22,25,32,51] As a result, the perturbation of Pt−Pt interactions by altering the stacking patterns of Pt(II) species in crystal lattices or in condensed phases can cause dramatic changes in color and emission.[1,22] From this point, many stimuli-responsive sensors have been developed based on Pt(II) complexes, such as vapochromic sensors,[14,15,25] solvochromic sensors,[22,24] ion sensors,[24,52] and sensors for biomolecules

and their conformational changes,[6,10,53] in which the architectures of Pt(II) complexes can be classified into four different types, including 1) cationic Pt(II) complexes;[6] 2) neutral Pt(II) complexes;[14] 3) Pt(II) double salts;[54] and 4) isolated binuclear complexes that allow stacking of planar Pt(II) moieties through metallophilic interactions.[23]

The simplest terpyridine-based Pt(II) complex, namely [Pt(tpy)Cl]X (tpy = 2,2':6',2''-terpyridine, X = anions), has been synthesized several decades ago, and its photophysical properties have been well investigated in the solid state.[55] Although the square planar $[Pt(tpy)Cl]^+$ monocations show a great variety of intermolecular Pt···Pt distances in different systems,[52,55-57] the use of this simple Pt(II) terpyridyl complex as a vapochromic and/or solvatochromic sensor was very rare. In 2008, Castellano and co-workers showed that [Pt(tpy)Cl]X (X = Cl^-, PF_6^-, or ClO_4^-) had color change and turn-on response in luminescence for several VOCs.[18] In the course of studying Pt(II) terpyridyl complexes, we also found that [Pt(tpy)Cl](PF_6) (**1**) displays a pronounced and reversible vapochromic response to acetonitrile. Due to the ease to study the $[Pt(tpy)Cl]^+$ system, we decided to focus on complex [Pt(tpy)Cl](PF_6) and use a combination of structural, spectroscopic and theoretical methods to get a better understanding of such phenomena.

Herein reported are the detailed studies of the vapochromism of **1**. Analyses of the crystal structures of **1** and **1**-MeCN provided interesting aspects on the basis of the structural effects in this system. The photophysical properties of **1** were investigated and interpreted by using time-dependent density functional theory (TDDFT) calculations, which demonstrated the important roles of Pt···Pt and terpyridyl π–π interactions in tuning the absorption properties of the $[Pt(tpy)Cl]^+$ aggregates. This combination of experimental and theoretical studies enables us to shed light on the key role of non-

covalent metal−metal interactions and π−π stacking in controlling the photophyscial properties of square-planar Pt(II) polypyridyl complexes.

Experimental Section

General methods and materials: Potassium tetrachloroplatinate(II), 2,2':6',2''-terpyridine, and ammonium hexafluorophosphate were obtained from Alfa Aesar. All other reagents were purchased from commercial suppliers and used as received unless otherwise noted. Dry solvents, including acetonitrile, acetone, dimethylformamide and diethyl ether, were purified by passage through activated alumina. Complex [Pt(tpy)Cl](PF$_6$) (**1**) was synthesized according to a published method.[55] Infrared spectra (2% sample in KBr) were recorded with a ThermoNicolet Avatar 360 spectrophotometer running the OMNIC software. ^{1}H NMR spectroscopic measurements were made on a Brüker spectrometer operating at 400 MHz. Powder X-ray diffraction measurements were made using a Shimadzu XRD−7000 diffractometer.

X-ray diffraction studies: Crystals of **1**-MeCN were grown by slow vapor diffusion of diethyl ether into a dilute acetonitrile solution of **1** at room temperature for a week. Crystals of **1** were grown either by slow vapor diffusion of diethyl ether into a dilute acetone solution of **1** at room temperature for 5 days or by slow evaporation of a concentrated DMF solution of **1** at room temperature for 2 months. Single crystals suitable for X-ray analysis were each coated with Paratone-N oil, suspended in a small fiber loop, and placed in a cooled gas stream on a Bruker APEX CCD X-ray

diffractometer. Diffraction intensities were measured using graphite monochromated Mo Kα radiation (λ = 0.71073 Å) at 153 (2) K and a combination of φ and ω scans traversing at 0.5° increments. Data collection, indexing, initial and final cell refinements, and frame integration were accomplished using APEX2 software.[58] The molecular structure of each complex was determined by direct methods and Fourier techniques and refined by full-matrix least squares. Absorption corrections were applied using the program SADABS.[59] Scattering factors and anomalous dispersion corrections were taken from the International Tables for X-ray Crystallography. Structure solution, refinement, graphic and generation of publication materials were performed by using SHELXTL, V6.14 software.[60]

Crystallographic studies revealed that the crystal structure of **1**-MeCN (CCDC-938348) is isomorphous with a previously reported hexafluoroantimonate congener (see below),[57] while the non-solvated form of **1** is the same as that reported previously.[52,57] In the structure of **1**-MeCN, each [Pt(tpy)Cl](PF$_6$) crystallizes with an acetonitrile solvent molecule. All non-hydrogen atoms were refined anisotropically. All hydrogen atoms binding to carbon were included into the model at geometrically calculated positions and refined using a riding model. The isotropic displacement parameters of all hydrogen atoms were fixed to 1.2 times the U value of the atoms they are linked to (1.5 times for methyl groups). Details of the data quality and a summary of the residual values of the refinements are listed in Table S1.

Titration and spectroscopic measurements: Absorption spectra were recorded using a UNICO scanning spectrophotometer (200−800 nm). Emission spectra were obtained using a HORIBA JY Fluoromax-4 fluorometer corrected for instrument response.

Monochromators were positioned with a 5-nm band-pass, and solution samples were degassed by at least three freeze-pump-thaw cycles before measurements. The titration experiments were measured using a concentrated stock solution of complex **1** in acetonitrile (3.30×10^{-4} M), which was further diluted to 1.65×10^{-5} M by different ratio of diethyl ether and acetonitrile.

Computational studies: The TDDFT calculations were carried out using Gaussian 09 program[61] with B3LYP functional and def-SV(P)[62] basis set. The dimeric and trimeric forms with the stack of two or three $[Pt(tpy)Cl]^+$ units along the axial direction were obtained from X-ray structures and were used for modeling. The lowest 100 singlet electronic excitation energies and their corresponding oscillator strengths were then calculated. On the basis of TDDFT results, the UV-vis spectra were analyzed using the SWizard program.[63,64] The solvent effect of acetonitrile was included by using the integral-equation-formalism polarizable continuum model.[65]

Results and Discussion

Synthesis and characterization: Complex $[Pt(tpy)Cl](PF_6)$ (**1**) was synthesized according to a published method,[55] and its identity and purity were confirmed by proton NMR and elemental analysis. The PF_6^- counteranion was suggested by FTIR showing two strong characteristic resonance peaks at 842 and 558 cm^{-1} (Figure S3).[66] Complex **1** is quite soluble in DMF and dimethyl sulfoxide, and has reasonable solubility in acetonitrile, acetone, methanol and other common polar organic solvents. Interestingly,

the yellow solids of **1** showed an instant color change to red upon exposure to either vapor or solution of acetonitrile. The resultant red form of **1** could turn back to its yellow form by drying the solid in vacuo or immersing it in other solvents, such as acetone, methanol and diethyl ether (Figure 1). These results suggest that complex **1** has reversible vapochromic features, and the interconversion between its red and yellow forms is depended on the presence or absence of acetonitrile.

Crystallographic studies: To get more information regarding the vapochromic feature of **1**, we analyzed the crystal structure of the non-solvated yellow form of **1** and the red form of **1**-MeCN. Crystallographic studies showed that the monocationic unit $[Pt(tpy)Cl]^+$ in both structures matched: each Pt atom is coordinated by three nitrogen atoms of the terpyridyl ligand and one terminal chloride atom to give a distorted square planar geometry (Figure 2); the Pt−N bond distances (2.019(5), 1.944(5), 2.015(5) Å) and the Pt−Cl bond length (2.323(3) Å) in **1**-MeCN are almost identical to those in **1**; the angles about the Pt centers do not show any significant variation, for example, the angle of N2−Pt1−Cl1 in **1**-MeCN is 178.70(17)°, nearly the same value as reported for **1**.[52,57] These results suggested that different colors of **1** were not caused by different coordination of the Pt atom, which was also consistent with the findings that the yellow and red forms of **1** had identical behaviors in solution measurements.

The $[Pt(tpy)Cl]^+$ units in the non-solvated yellow form of **1** in triclinic space group $P\bar{1}$ form an one-dimensional line along the *b* axis in a head-to-tail arrangement. The intermolecular Cl···H−C distances at 2.794 Å as shown in Figure 3a is considerably shorter than the sum of van der Waals radii of hydrogen and chlorine atoms (1.20 + 1.75

= 2.95 Å), which is indicative of weak interactions between the two adjacent $[Pt(tpy)Cl]^+$ units. This kind of weak interactions plays an important role in crystal packing and is well documented in the literature.[19,25,32,49,50] In addition to this Cl···H−C interaction, counteranion PF_6^- is also crucial for the formation of such 1D lines by connecting two $[Pt(tpy)Cl]^+$ units through many weak intermolecular F···H−C interactions (the sum of van der Waals radii of hydrogen and fluorine atoms is 1.20 + 1.47 = 2.67 Å).

The packing of such 1D lines through weak F···H−C contacts and electrostatic interactions affords a 2D array with Pt···Pt separations at 10.027 and 13.766 Å in the directions of *b* and *c* axes, respectively. These 2D arrays further stack in an alternating ABAB… fashion with A and B planes in the opposite orientation to give a 3D structure. As shown in Figure 3c, there are two kinds of Pt···Pt distances alternating in this 3D arrangement (4.032 and 3.340 Å). Because the van der waals radius of Pt is 1.75 Å, it is suggested that intermolecular interactions are largely confined within the two metal centers that have a short Pt···Pt distance (see below).

The red form **1**-MeCN crystallized in orthorhombic space group *Pnma* with unit cell parameters summarized in Table 1. In contrast to **1**, there is a co-crystallized acetonitrile solvent molecule per **1** in the X-ray structure of **1**-MeCN, which is consistent with our FTIR studies showing a −C≡N bond stretch at 2251 cm^{-1}. The $[Pt(tpy)Cl]^+$ units in **1**-MeCN form an 1D line along the *c* axis in a similar head-to-tail arrangement. In addition to intermolecular Cl···H−C and F···H−C interactions, the acetonitrile molecule is suggested to contribute to the formation of such a 1D line through interactions between the nitrogen atom and the terpyridyl ligand backbone and also interactions between the PF_6^- anion and the methyl group of acetonitrile (Figure 4a, the van der Waals radius of

nitrogen is 1.55 Å). However, unlike the structure of **1** in which the 1D lines pack in the same direction in a 2D array, in the structure of **1**-MeCN, these 1D lines have two opposite orientations and assemble in an alternating way to give a 2D array with Pt···Pt separations at 10.766 and 14.416 Å in the directions of *c* and *a* axes, respectively.

The zigzag configuration of the 2D array in **1**-MeCN is therefore different to that found in **1**. Weak interactions between PF_6^- anions and acetonitrile molecules are proposed to assist the formation of such an alternating arrangement (Figure 4a). In addition, the stack of these 2D arrays in an alternating opposite orientation through intermolecular π–π stacking and Pt···Pt interactions resulted in a 3D structure with a similar ABAB… fashion (Figure 4c). Compared to **1**, the metal–metal interactions in **1**-MeCN is largely extended to a much linear chain-like array of Pt atoms with a short Pt···Pt distance at 3.362 Å (the Pt-Pt-Pt angle in **1**-MeCN is 157.18°, while it is 137.68° in **1**). This structural feature of **1**-MeCN is suggested to be the origin of its unique photophysical properties in comparison with the yellow form of **1** (see below).

Closer examinations of the X-ray crystal structures of **1** and **1**-MeCN may shed light on the role of acetonitrile in controlling the packing of $[Pt(tpy)Cl]^+$ units in crystal lattices. As shown in Figure 5a and 5b, in the X-ray crystal structure of **1**, the PF_6^- anion is located outside the $[Pt(tpy)Cl]^+$ plane due to the small space between two neighboring $[Pt(tpy)Cl]^+$ units along the *b* axis. This displacement of PF_6^- anions out of the $[Pt(tpy)Cl]^+$ plane results in two alternating Pt···Pt distances: a short distance at 3.340 Å without interlamellar PF_6^- anions and a long distance at 4.032 Å with interlamellar PF_6^- anions. However, in the structure of **1**-MeCN, an acetonitrile molecule inserts into the gap between two $[Pt(tpy)Cl]^+$ units (Figure 5c) because of its linear shape and an

appropriate size as we did not observe similar vapochromic response of **1** using other nitriles, including benzonitrile and propionitrile. Weak interactions between the nitrogen atom of an acetonitrile and hydrogen atoms of terpyridyl ligands (as mentioned above) might be also the driving force for this insertion. This structural change pushes the two neighboring $[Pt(tpy)Cl]^+$ units away from each other, for example, the Pt···Pt distance along *b* axis in **1** is 10.03 Å, while it is 10.77 Å along *c* axis in **1**-MeCN. With an expanded cavity in **1**-MeCN for PF_6^- anions, they are now located perfectly on the $[Pt(tpy)Cl]^+$ plane (Figure 5d). Because of the absence of interlamellar PF_6^- anions, the intermolecular Pt···Pt separation is short at 3.362 Å in **1**-MeCN.

The yellow and red forms of **1** were further characterized by powder X-ray diffraction (PXRD) methods. Different yellow samples of **1** obtained either from direct crystallization of $[Pt(tpy)Cl](PF_6)$ from acetone or DMF or from drying red crystals of **1**-MeCN in vacuo gave nearly the same PXRD pattern, which matched the calculated one using the single crystal X-ray structure of **1** (Figure S4). After exposing solids of **1** to the vapor of acetonitrile, the color turned from yellow to red, and the PXRD pattern changed to be very similar to that of **1**-MeCN. It is worthy mentioning that if the conversion upon exposure to acetonitrile was not complete, PXRD data showed a mixture of both **1** and **1**-MeCN.

Electronic absorption and emission studies: The photophysical properties of **1** were investigated in solution and solid states. As shown in Figure S1, a highly diluted acetonitrile solution of **1** (1.65×10^{-5} M) gradually turned from colorless to pink upon increasing diethyl ether content. We rationalized that the addition of diethyl ether to the

acetonitrile solution of **1** would decrease its solubility, and the aggregation of **1** in solution was responsible for this color change. Similar phenomena were also observed in other Pt(II) polypyridyl complexes.[1,22,24,26] This process was studied in detail using titration experiments. When the content of diethyl ether in a mixture of Et_2O:MeCN was below 78% (v/v), the UV-vis spectrum of **1** showed a weak absorption between 360−440 nm with a maximum at 387 nm, which could be assigned to a metal-to-ligand charge transfer (MLCT) band. The strong absorption between 200−360 nm originates from spin-allowed intraligand transitions (i.e. π−π*) of the terpyridyl ligand ($> 2 \times 10^4$ M^{-1} cm^{-1}).

When the content of diethyl ether reached 78%, a new absorption band between 450−580 nm appeared with a maximum at 518 nm (Figure 6a), which is consistent with the aggregation of **1** in the diethyl ether−acetonitrile system.[1,22,24,26,67] This resultant solution remained clear overnight with no precipitation. Further increase of the diethyl ether content up to 88% caused the continuing enhancement of the absorption between 450−580 nm concomitant with the constant decrease of the absorption between 200−360 nm. When the diethyl ether content was more than 88%, red precipitates of **1** started to form, which caused the oscillation of the spectrum (Figure S2). In contrast to the acetonitrile solution of **1**, addition of diethyl ether to either DMF or acetone solution of **1** did not cause detectable increase of absorption in the visible light range. The UV-vis spectra of **1** in acetonitrile with the increment of concentration of **1** showed an agreement with Beer's law (Figure S5), which indicated that such aggregation was not likely to take place in our studies possibly due to the limited solubility of **1** in acetonitrile.

Accordingly, this titration experiment was also monitored using emission spectroscopy. When the diethyl ether content was below 78%, the acetonitrile solution of

1 showed no appreciable emission band at room temperature using an excitation at 500 nm. However, a weak emission band between 525−800 nm (no data were collected above 800 nm due to the detection limit of our instrument) with a maximum at 702 nm started to grow up at the point of 78% diethyl ether content. Significantly, the emission intensity constantly increased with the increase of the diethyl ether content (Figure 6b).

The emission properties of **1** were further investigated in the solid state during vapochromic response. In the absence of acetonitrile vapor, the yellow form of **1** (Figure 7) emitted between 500−800 nm with a maximum at 632 nm by excitation at 450 nm (Figure 8), which was the typical emission of triplet MLCT band in Pt(II) terpyridyl systems.[55] When this yellow solid was exposed to acetonitrile vapor, it slowly changed color from yellow to red (Figure 7). The resulted red solid therefore showed an emission band between 550−850 with a maximum at 752 nm (Figure 8), corresponding to the emission from triplet MMLCT character in the solid state (see below). This solid-state luminescence is similar to the abovementioned emission observed in the titration experiments. These results indicate that the packing of $[Pt(tpy)Cl]^+$ units changes in the solid state of **1** upon exposure to acetonitrile vapor. Importantly, the red form of **1** could be again turned back to its yellow form by drying the solid in vacuo, and this process could be repeated many times without substantial chemical degradation of the sample, indicating its good reversibility of vapochromism. Figure 7 shows the reversibility of this vapochromic process for ten cycles. There is no significant change in the emission spectra for the same colored materials of **1**.

Theoretical studies: TDDFT calculations were carried out to better understand the nature of the photophysical properties of **1**. The dimeric and trimeric structures with the stack of either two or three $[Pt(tpy)Cl]^+$ units along the axial direction, obtained from the X-ray structures of **1**-MeCN and **1**, were used as models to elucidate the importance of Pt···Pt and terpyridyl π–π interactions in affecting the absorption features. The effect of the counterion PF_6^- was also investigated. Here we focus the discussion on the visible light range, which directly affects the perceived color of different forms of **1**. Some important singlet transitions are listed in Table 2, while the full dataset are given in Table S3-S7.

The absorption spectra of dimers of $[Pt(tpy)Cl]^+$ (taken from **1**-MeCN; Pt···Pt distance at 3.362 Å) with and without PF_6^- counterions were first calculated. As shown in Figure 9, their absorptions were almost identical, indicating that the effect of PF_6^- counterion is negligible. In addition, the calculated absorption bands of $[Pt(tpy)Cl]^+$, with strong oscillator strengths located in the region of 200-350 nm, is consistent with experimental results observed in a 5:5:1 EtOH:MeOH:DMF (EMD) solution by Gray et al.[55] It is necessary to point out that, in our calculations, a very weak absorption band at 515 nm was in an excellent agreement with a weak band at 510 nm for 0.15 mM $[Pt(tpy)Cl](PF_6)$ in the EMD glassy mixture at 77 K.[55] Interestingly, this band at 510 nm disappeared upon increasing the temperature of the solution, probably due to the destroy of the $\{[Pt(tpy)Cl]^+\}_2$ dimeric structure at room temperature. Analysis of the molecular orbitals (MOs) of $\{[Pt(tpy)Cl]^+\}_2$ showed that the orbitals interacting most strongly were those extending perpendicularly to the molecular plane of the $[Pt(tpy)Cl]^+$ units (d_{xz}, d_{yz}, and d_{z2}), and they could be split into bonding and antibonding combinations: σ_d and σ_d*

orbitals for d_{z^2}, and π_d and π_d^* for d_{xz} (and d_{yz}) using a simplified MO model (Figure 10a).[51,68,69] It should be pointed out that the d orbitals of the Pt center strongly mixed with the 3p orbitals of the Cl ligand. For simplicity, we will still use the d(Pt) to represent such hybrid orbitals. As shown in Figure 10b, the highest occupied molecular orbital (HOMO) is antibonding σ_d^* orbital, while HOMO-1 and HOMO-2 are π_d^* and π_d orbitals which have significant contribution of Pt d_{xz} orbitals. As such, all these three orbitals are arising from Pt···Pt interactions. The lowest unoccupied molecular orbital (LUMO), LUMO+1 and LUMO+2 show the contributions of π^* orbitals of each terpyridine ligand, suggesting the presence of terpyridyl $\pi-\pi$ interactions. Our TDDFT calculations confirmed the contributions of these orbitals to the visible absorptions in the dimeric structure (Table 2). In other words, the electronic absorptions of $[Pt(tpy)Cl]^+$ dimers in the visible light range are associated with metal-metal-to-ligand charge transfer (MMLCT) transitions arising from terpyridyl $\pi-\pi$ and Pt···Pt interactions.

The TDDFT calculations were carried out also using trimeric structures in the gas phase to elucidate the geometry effect on the absorption properties of **1**. As mentioned above, in the structure of **1**, there are two kinds of Pt···Pt nearest-neighbor distances, 4.032 and 3.340 Å. While in **1**-MeCN, intermolecular Pt···Pt distances are the same (3.362 Å). It can be seen from Figure 11 that the lowest energy absorption band shows a maximum peak at 550 nm for **1**-MeCN and 474 nm for **1**. In both cases, the visible absorption peak was found to be ascribed to the $\sigma_d^* \rightarrow \pi^*$(tpy) transition.

However, as shown in Figure 12a, the σ_d^* orbital (HOMO-6) arising from the d_{z^2} orbitals of Pt was extended to all three subunits in **1**-MeCN. On the other hand, the MO diagrams of the trimeric structures in **1** showed that the metal−metal interaction, raised

from overlap of filled d orbitals between the adjacent $[Pt(tpy)Cl]^+$ units along the axial direction, was presented only in the two metal centers with a short Pt···Pt distance (such as HOMO-11 and HOMO-8 in Figure 12b). Therefore, the metal−metal interaction in **1**-MeCN destabilizes the antibonding σ_d*(Pt) orbital but stabilizes the π*(tpy) orbital, and as a result, lowers the energy of σ_d*(Pt) → π*(tpy) transition in Pt-tpy systems and causes a dramatic red shift in absorption spectroscopy.

The packing of $[Pt(tpy)Cl]^+$ in other anion systems: Structural comparison between X-ray structures of [Pt(tpy)Cl]X (X = PF_6, SbF_6, ClO_4, Cl) further corroborates the key role of the packing of $[Pt(tpy)Cl]^+$ in their photophysical properties. Doerrer and co-workers reported the synthesis and structural characterization of [Pt(tpy)Cl](SbF_6) (**2**) and several other derivatives and performed a careful structural comparison between these solids.[57] As an analogue of **1**, both the non-solvated yellow form and the red form of **2** with an acetonitrile solvate molecule could be isolated (Figure S6, crystal growth was followed by the published method). Crystal **2**-MeCN is isomorphous to **1**-MeCN with nearly identical unit cell parameters, but the non-solvated yellow form of **2** crystallizes in monoclinic space group $P2_1/c$ and is different to **1**, which crystallizes in $P\bar{1}$. As we expected, in the X-ray structure of **2**-MeCN, $[Pt(tpy)Cl]^+$ units stack to give an extended chain-like array of Pt atoms with a short Pt···Pt distance at 3.372 Å (Figure S7), while in the yellow form of **2**, there are two alternating Pt···Pt distances (4.035 and 3.342 Å). Attempts to examine the vapochromic feature of **2** showed that its yellow form could also turn to red upon exposure to the vapor of acetonitrile, but this change was much slower

compared to that of **1**. This difference may be caused by different packing of $[Pt(tpy)Cl]^+$ in the non-solvated forms of **1** and **2** (Figure S8).

Similar to **1** and **2**, the packing of $[Pt(tpy)Cl]^+$ affects the photophysical properties of complexes $[Pt(tpy)Cl](ClO_4)$ (**3**)[52,55] and [Pt(tpy)Cl]Cl (**4**).[56] For **3**, there are an orange form with alternating long and short Pt···Pt distances of 4.197 and 3.269 Å and a red form with short Pt···Pt distances of 3.303 and 3.369 Å; for **4**, there are a yellow form with alternating long and short Pt···Pt distances of 4.327 and 3.390 Å and a red form with short Pt···Pt distances of 3.315 and 3.436 Å. These findings are consistent with our theoretical results that the extension of $\{[Pt(tpy)Cl]^+\}_2$ dimeric units through short Pt···Pt distances can considerably lower the transition energy of MMLCT and thus cause a dramatic red shift in electronic absorption spectroscopy.

Conclusion

The simplest Pt(II) terpyridyl complex $[Pt(tpy)Cl](PF_6)$ (**1**) was shown to have a reversible response in color and emission to acetonitrile. Light yellow form of **1** turned to red upon exposure to either vapor or solution of acetonitrile, concomitant with a change in luminescence from 632 nm to 752 nm. Crystallographic analyses on X-ray structures of **1**-MeCN and **1** reported previously revealed that these photophysical differences were not caused by the coordination of acetonitrile to the Pt(II) center in **1**-MeCN but were a result of different packing of square-planar $[Pt(tpy)Cl]^+$ units controlled by co-crystallized acetonitrile molecules: **1**-MeCN has an extended chain-like array of Pt atoms with a short Pt···Pt distance at 3.362 Å; while in **1**, there are two alternating Pt···Pt

distances (4.032 and 3.340 Å). Titration studies showed that two electronic absorption bands in the visible light range at 473 and 518 nm and an emission band at 702 nm grew up by increasing the diethyl ether content of an acetonitrile solution of **1**, a process not observed from the solution of DMF and acetone. TDDFT calculations demonstrated that metal−metal and terpyridyl π−π interactions play important roles in tuning the absorption properties of the $[Pt(tpy)Cl]^+$ system. The stack of three molecules of **1** with a short Pt···Pt distance lowers the transition energy of σ_d*(Pt) → π*(tpy) in Pt-tpy systems, compared to the dimer or the trimer of **1** with an alternating short and long Pt···Pt distances. This change in electronic structures is consistent with a dramatic red shift in UV-vis spectroscopy and a significant growth of absorption in the visible light range.

Acknowledgements. We are grateful to the support from the "Young Thousand Talents Program" in China and the National Science Foundation of China under grant no. 21101170 (to R. C.), no. 21271166 (to P. D.) and no. 21203245 (to W. L.). We thank Dr. Xiang Hao at the Center for Physicochemical Analysis and Measurement, Institute of Chemistry, Chinese Academy of Sciences, for single crystal X-ray diffraction data collection.

Supporting Information. Crystal data and structure refinement parameters; FTIR and UV-vis spectra; powder X-ray diffraction data; X-ray data as CIF file for **1**-MeCN; calculated singlet excited-states transitions. This material is available free of charge via

the Internet at http://pubs.rsc.org.

References

1. K. M. C. Wong and V. W. W. Yam, *Acc. Chem. Res.*, 2011, **44**, 424-434.
2. J. S. Wu, W. M. Liu, J. C. Ge, H. Y. Zhang and P. F. Wang, *Chem. Soc. Rev.*, 2011, **40**, 3483-3495.
3. J. F. Zhang, Y. Zhou, J. Yoon and J. S. Kim, *Chem. Soc. Rev.*, 2011, **40**, 3416-3429.
4. X. Q. Chen, X. Z. Tian, I. Shin and J. Yoon, *Chem. Soc. Rev.*, 2011, **40**, 4783-4804.
5. J. Z. Zhao, S. M. Ji, W. H. Wu, W. T. Wu, H. M. Guo, J. F. Sun, H. Y. Sun, Y. F. Liu, Q. T. Li and L. Huang, *Rsc Adv.*, 2012, **2**, 1712-1728.
6. C. Yu, K. M. C. Wong, K. H. Y. Chan and V. W. W. Yam, *Angew. Chem. Int. Ed.*, 2005, **44**, 791-794.
7. R. Hu, J. Feng, D. H. Hu, S. Q. Wang, S. Y. Li, Y. Li and G. Q. Yang, *Angew. Chem. Int. Ed.*, 2010, **49**, 4915-4918.
8. Y. Liu, Y. H. Tang, N. N. Barashkov, I. S. Irgibaeva, J. W. Y. Lam, R. R. Hu, D. Birimzhanova, Y. Yu and B. Z. Tang, *J. Am. Chem. Soc.*, 2010, **132**, 13951-13953.
9. Y. Liu, C. M. Deng, L. Tang, A. J. Qin, R. R. Hu, J. Z. Sun and B. Z. Tang, *J. Am. Chem. Soc.*, 2011, **133**, 660-663.
10. C. Y. S. Chung and V. W. W. Yam, *J. Am. Chem. Soc.*, 2011, **133**, 18775-18784.

11. C. F. Ke, H. Destecroix, M. P. Crump and A. P. Davis, *Nature Chem.*, 2012, **4**, 718-723.

12. L. G. Beauvais, M. P. Shores and J. R. Long, *J. Am. Chem. Soc.*, 2000, **122**, 2763-2772.

13. J. Pang, E. J. P. Marcotte, C. Seward, R. S. Brown and S. N. Wang, *Angew. Chem. Int. Ed.*, 2001, **40**, 4042-4045.

14. C. E. Buss and K. R. Mann, *J. Am. Chem. Soc.*, 2002, **124**, 1031-1039.

15. R. C. Bailey and J. T. Hupp, *J. Am. Chem. Soc.*, 2002, **124**, 6767-6774.

16. L. J. Grove, J. M. Rennekamp, H. Jude and W. B. Connick, *J. Am. Chem. Soc.*, 2004, **126**, 1594-1595.

17. M. J. Katz, T. Ramnial, H. Z. Yu and D. B. Leznoff, *J. Am. Chem. Soc.*, 2008, **130**, 10662-10673.

18. M. L. Muro, C. A. Daws and F. N. Castellano, *Chem. Commun.*, 2008, 6134-6136.

19. J. Ni, Y. H. Wu, X. Zhang, B. Li, L. Y. Zhang and Z. N. Chen, *Inorg. Chem.*, 2009, **48**, 10202-10210.

20. M. Albrecht, M. Lutz, A. L. Spek and G. van Koten, *Nature*, 2000, **406**, 970-974.

21. M. Albrecht, R. A. Gossage, M. Lutz, A. L. Spek and G. van Koten, *Chem. Eur. J.*, 2000, **6**, 1431-1445.

22. V. W. W. Yam, K. M. C. Wong and N. Y. Zhu, *J. Am. Chem. Soc.*, 2002, **124**, 6506-6507.

23. M. Kato, A. Omura, A. Toshikawa, S. Kishi and Y. Sugimoto, *Angew. Chem. Int. Ed.*, 2002, **41**, 3183-3185.

24. V. W. W. Yam, K. H. Y. Chan, K. M. C. Wong and N. Y. Zhu, *Chem. Eur. J.*, 2005, **11**, 4535-4543.

25. S. C. F. Kui, S. S. Y. Chui, C. M. Che and N. Y. Zhu, *J. Am. Chem. Soc.*, 2006, **128**, 8297-8309.

26. C. Po, A. Y. Y. Tam, K. M. C. Wong and V. W. W. Yam, *J. Am. Chem. Soc.*, 2011, **133**, 12136-12143.

27. J. R. Stork, M. M. Olmstead and A. L. Balch, *J. Am. Chem. Soc.*, 2005, **127**, 6512-6513.

28. T. Abe and K. Shinozaki, *Inorg. Chem.*, 2005, **44**, 849-851.

29. K. A. McGee, B. J. Marquardt and K. R. Mann, *Inorg. Chem.*, 2008, **47**, 9143-9145.

30. Z. W. Liu, Z. Q. Bian, J. Bian, Z. D. Li, D. B. Nie and C. H. Huang, *Inorg. Chem.*, 2008, **47**, 8025-8030.

31. I. M. Sluch, A. J. Miranda and L. M. Slaughter, *Cryst. Growth Des.*, 2009, **9**, 1267-1270.

32. T. J. Wadas, Q. M. Wang, Y. J. Kim, C. Flaschenreim, T. N. Blanton and R. Eisenberg, *J. Am. Chem. Soc.*, 2004, **126**, 16841-16849.

33. V. W. W. Yam, K. H. Y. Chan, K. M. C. Wong and B. W. K. Chu, *Angew. Chem. Int. Ed.*, 2006, **45**, 6169-6173.

34. A. L. Grzesiak and A. J. Matzger, *Inorg. Chem.*, 2007, **46**, 453-457.

35. R. Pattacini, C. Giansante, P. Ceroni, M. Maestri and P. Braunstein, *Chem. Eur. J.*, 2007, **13**, 10117-10128.

36. J. Forniés, S. Fuertes, J. A. López, A. Martín and V. Sicilia, *Inorg. Chem.*, 2008, **47**, 7166-7176.

37. L. J. Grove, A. G. Oliver, J. A. Krause and W. B. Connick, *Inorg. Chem.*, 2008, **47**, 1408-1410.

38. P. Du, J. Schneider, W. W. Brennessel and R. Eisenberg, *Inorg. Chem.*, 2008, **47**, 69-77.

39. H. V. R. Dias, H. V. K. Diyabalanage, M. A. Rawashdeh-Omary, M. A. Franzman and M. A. Omary, *J. Am. Chem. Soc.*, 2003, **125**, 12072-12073.

40. M. M. Olmstead, F. L. Jiang, S. Attar and A. L. Balch, *J. Am. Chem. Soc.*, 2001, **123**, 3260-3267.

41. R. L. White-Morris, M. M. Olmstead, F. L. Jiang, D. S. Tinti and A. L. Balch, *J. Am. Chem. Soc.*, 2002, **124**, 2327-2336.

42. R. L. White-Morris, M. M. Olmstead and A. L. Balch, *J. Am. Chem. Soc.*, 2003, **125**, 1033-1040.

43. E. J. Fernández, J. M. López-de-Luzuriaga, M. Monge, M. E. Olmos, J. Pérez, A. Laguna, A. A. Mohamed and J. P. Fackler Jr., *J. Am. Chem. Soc.*, 2003, **125**, 2022-2023.

44. J. Lefebvre, R. J. Batchelor and D. B. Leznoff, *J. Am. Chem. Soc.*, 2004, **126**, 16117-16125.

45. K. M. C. Wong, L. L. Hung, W. H. Lam, N. Y. Zhu and V. W. W. Yam, *J. Am. Chem. Soc.*, 2007, **129**, 4350-4365.

46. E. J. Fernández, J. M. López-de-Luzuriaga, M. Monge, M. E. Olmos, R. C. Puelles, A. Laguna, A. A. Mohamed and J. P. Fackler Jr., *Inorg. Chem.*, 2008, **47**, 8069-8076.

47. V. K. M. Au, K. M. C. Wong, D. P. K. Tsang, M. Y. Chan, N. Y. Zhu and V. W. W. Yam, *J. Am. Chem. Soc.*, 2010, **132**, 14273-14278.

48. S. Das and P. K. Bharadwaj, *Inorg. Chem.*, 2006, **45**, 5257-5259.

49. J. S. Field, L. P. Ledwaba, O. Q. Munro and D. R. McMillin, *CrystEngComm*, 2008, **10**, 740-747.

50. W. Lu, M. C. W. Chan, N. Y. Zhu, C. M. Che, Z. K. He and K. Y. Wong, *Chem. Eur. J.*, 2003, **9**, 6155-6166.

51. C. Garino, E. Gallo, N. Smolentsev, P. Glatzel, R. Gobetto, C. Lamberti, P. J. Sadler and L. Salassa, *Phys. Chem. Chem. Phys.*, 2012, **14**, 15278-15281.

52. S. D. Taylor, W. Howard, N. Kaval, R. Hart, J. A. Krause and W. B. Connick, *Chem. Commun.*, 2010, **46**, 1070-1072.

53. C. Yu, K. H. Y. Chan, K. M. C. Wong and V. W. W. Yam, *Proc. Natl. Acad. Sci. USA*, 2006, **103**, 19652-19657.

54. S. M. Drew, D. E. Janzen, C. E. Buss, D. I. MacEwan, K. M. Dublin and K. R. Mann, *J. Am. Chem. Soc.*, 2001, **123**, 8414-8415.

55. J. A. Bailey, M. G. Hill, R. E. Marsh, V. M. Miskowski, W. P. Schaefer and H. B. Gray, *Inorg. Chem.*, 1995, **34**, 4591-4599.

56. C. S. Angle, A. G. DiPasquale, A. L. Rheingold and L. H. Doerrer, *Acta Cryst.*, 2006, **C62**, 340-342.

57. V. Phillips, F. G. Baddour, T. Lasanta, J. M. López-de-Luzuriaga, J. W. Bacon, J. A. Golen, A. L. Rheingold and L. H. Doerrer, *Inorg. Chim. Acta*, 2010, **364**, 195-204.

58. *APEX2 v2009*, Bruker AXS., Madison, WI, 2009.

59. G. M. Sheldrick, *SADABS, 2008/1*, University of Göttingen, Göttingen, Germany, 2008.

60. G. M. Sheldrick, *Acta Cryst.*, 2008, **A64**, 112-122.

61. M. J. Frisch, G. W. Trucks, H. B. Schlegel, G. E. Scuseria, M. A. Robb, J. R. Cheeseman, G. Scalmani, V. Barone, B. Mennucci, G. A. Petersson, H. Nakatsuji, M. Caricato, X. Li, H. P. Hratchian, A. F. Izmaylov, J. Bloino, G. Zheng, J. L. Sonnenberg, M. Hada, M. Ehara, K. Toyota, R. Fukuda, J. Hasegawa, M. Ishida, T. Nakajima, Y. Honda, O. Kitao, H. Nakai, T. Vreven, J. A. J. Montgomery, J. E. Peralta, F. Ogliaro, M. Bearpark, J. J. Heyd, E. Brothers, K. N. Kudin, V. N. Staroverov, T. Keith, R. Kobayashi, J. Normand, K. Raghavachari, A. Rendell, J. C. Burant, S. S. Iyengar, J. Tomasi, M. Cossi, N. Rega, N. J. Millam, M. Klene, J. E. Knox, J. B. Cross, V. Bakken, C. Adamo, J. Jaramillo, R. Gomperts, R. E. Stratmann, O. Yazyev, A. J. Austin, R. Cammi, C. Pomelli, J. W. Ochterski, R. L. Martin, K. Morokuma, V. G. Zakrzewski, G. A. Voth, P. Salvador, J. J. Dannenberg, S. Dapprich, A. D. Daniels, Ö. Farkas, J. B. Foresman, J. V. Ortiz, J. Cioslowski and D. J. Fox, *Gaussian 09 (Revision A.02)*, Gaussian, Inc., Wallingford, CT, 2010.

62. A. Schäfer, H. Horn and R. Ahlrichs, *J. Chem. Phys.*, 1992, **97**, 2571-2577.

63. S. I. Gorelsky, *SWizard Program*, 2012.

64. S. I. Gorelsky and A. B. P. Lever, *J. Organomet. Chem.*, 2001, **635**, 187-196.

65. J. Tomasi, B. Mennucci and E. Cancès, *J. Mol. Struc. THEOCHEM*, 1999, **464**, 211-226.

66. R. Cao, B. D. McCarthy and S. J. Lippard, *Inorg. Chem.*, 2011, **50**, 9499-9507.

67. A. M. Krause-Heuer, N. J. Wheate, W. S. Price and J. Aldrich-Wright, *Chem. Commun.*, 2009, 1210-1212.

68. K. Krogmann, *Angew. Chem. Int. Ed.*, 1969, **8**, 35-42.

69. A. Dedieu, *Chem. Rev.*, 2000, **100**, 543-600.

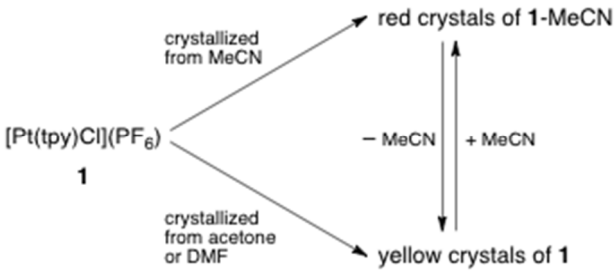

Figure 1. Schematic illustration showing the interconversion of red and yellow forms of **1** upon the loss of or the exposure to acetonitrile.

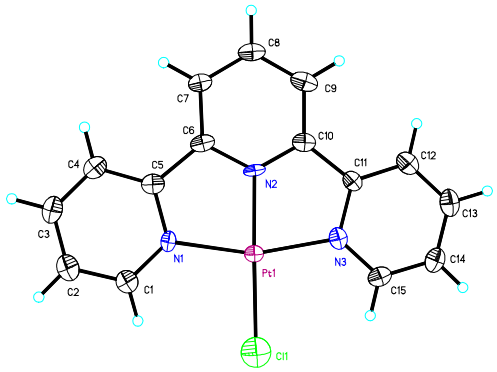

Figure 2. Thermal ellipsoid plot (50% probability) of the X-ray structure of **1**-MeCN. Counterion PF_6^- and co-crystallized solvent acetonitrile are omitted.

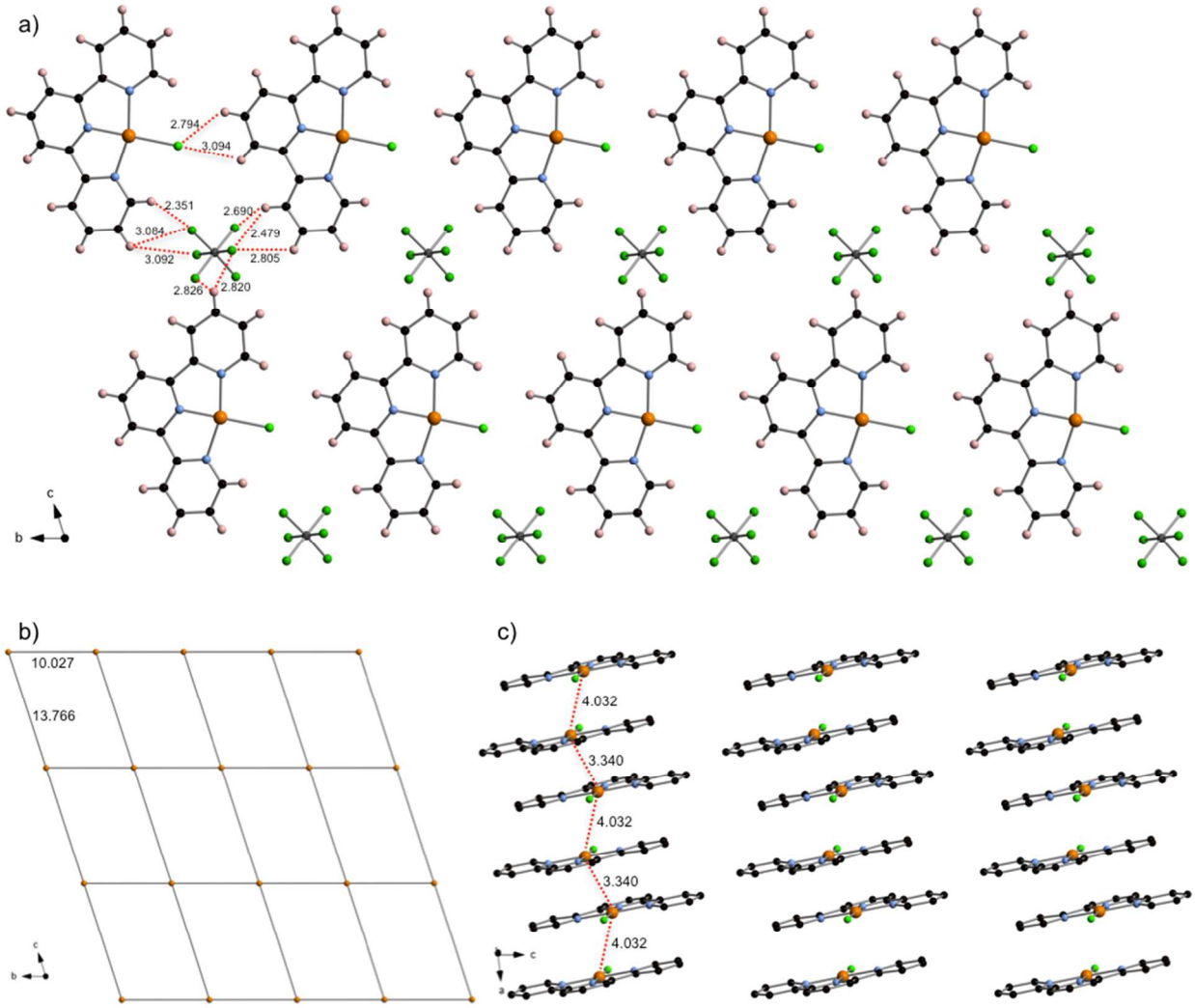

Figure 3. Ball-and-stick representations of the X-ray structure of **1** showing its a) 1D line, b) 2D array and c) 3D stack. Some of weak Cl···H−C and F···H−C interactions are indicated. All distances are in Å. The C, N, H, Cl, F, P and Pt atoms are depicted in black, light blue, light pink, light green, green, gray and orange, respectively.

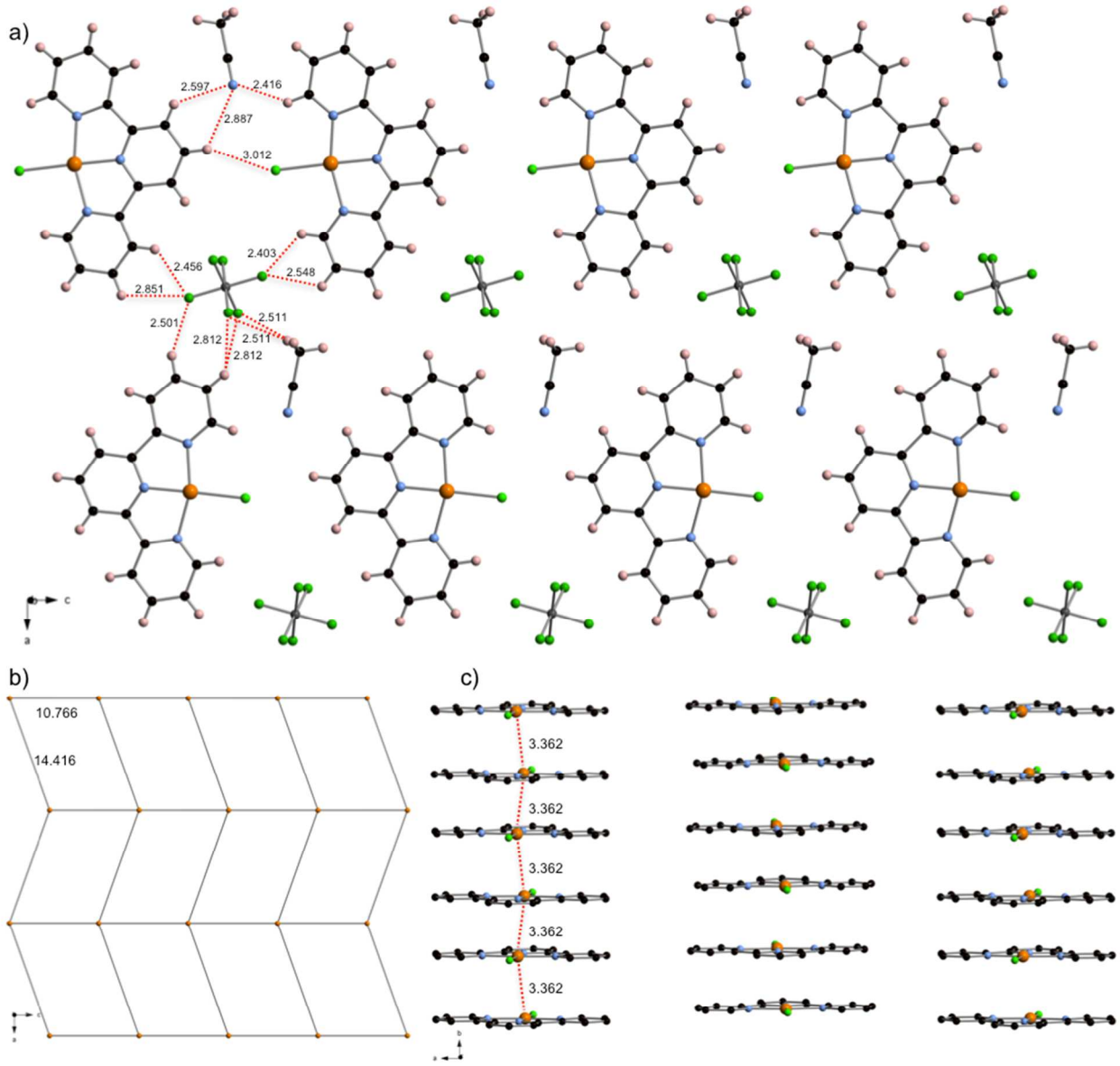

Figure 4. Ball-and-stick representations of the X-ray structure of **1**-MeCN showing its a) 1D line, b) 2D array and c) 3D stack. Some of weak Cl···H−C, F···H−C and N···H−C interactions are indicated. All distances are in Å. The C, N, H, Cl, F, P and Pt atoms are depicted in black, light blue, light pink, light green, green, gray and orange, respectively.

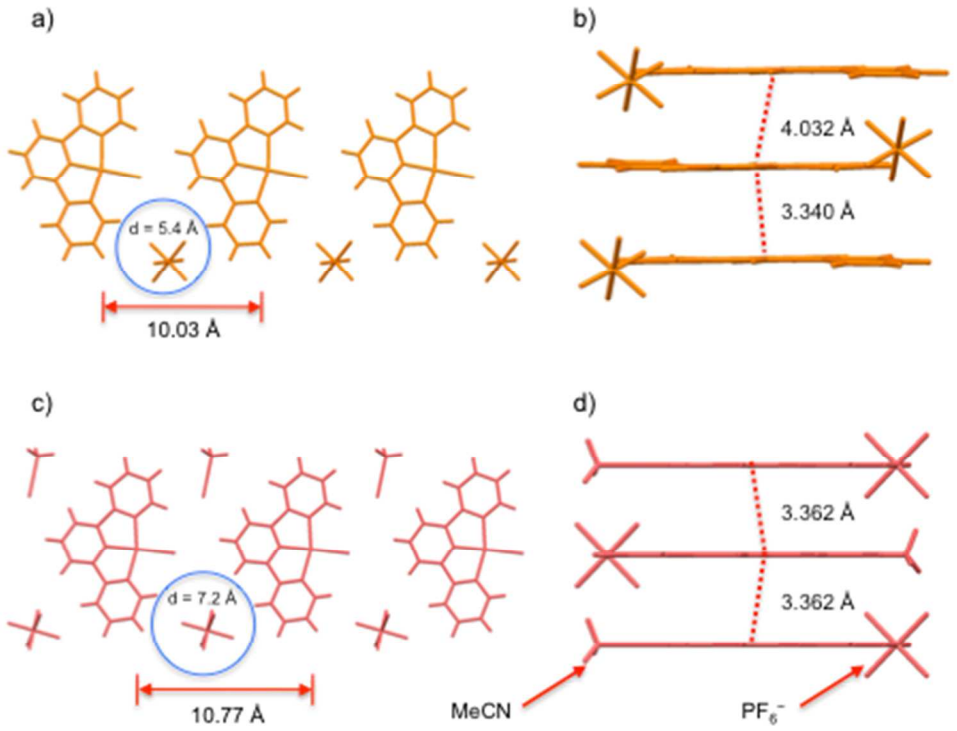

Figure 5. X-ray structures of **1** (a and b) and **1**-MeCN (c and d). In the structure of **1**, the PF_6^- anion is located outside the $[Pt(tpy)Cl]^+$ plane due to the small space between two $[Pt(tpy)Cl]^+$ units along the *b* axis; while in the structure of **1**-MeCN, the PF_6^- anion is located on the $[Pt(tpy)Cl]^+$ plane because the insertion of an acetonitrile molecule between two $[Pt(tpy)Cl]^+$ units expands this cavity.

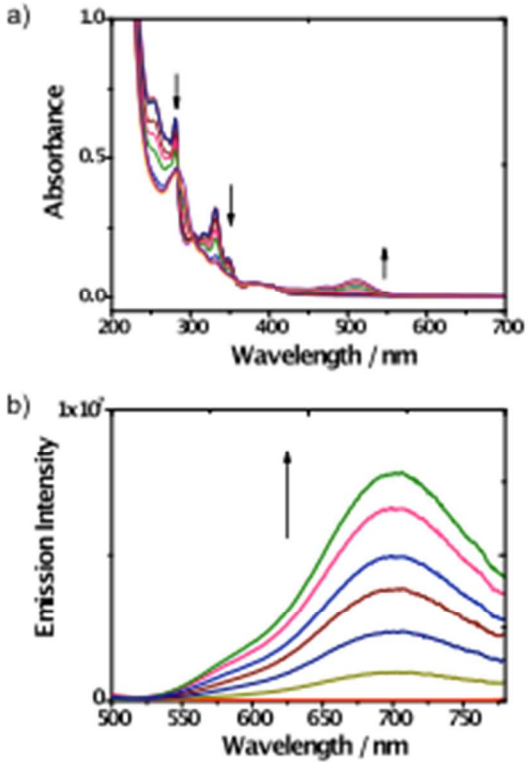

Figure 6. a) Electronic absorption spectra of **1** (1.65×10^{-5} M) in acetonitrile upon increasing Et_2O content. b) Emission spectra of **1** (1.65×10^{-5} M) in acetonitrile upon increasing Et_2O content. The Et_2O content increases as follows: 72%, 78%, 80%, 82%, 84%, 86%, 88% (v/v).

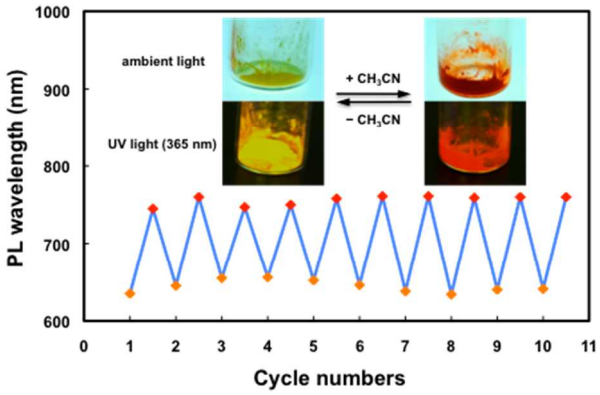

Figure 7. Color change of **1** upon exposure to acetonitrile and the reversibility of this vapochromic response. The maximum emission intensity of the red form (λ_{em}^{max} = 752 nm) and the yellow form (λ_{em}^{max} = 632 nm) *vs* cycle numbers. The excitation wavelength is 450 nm.

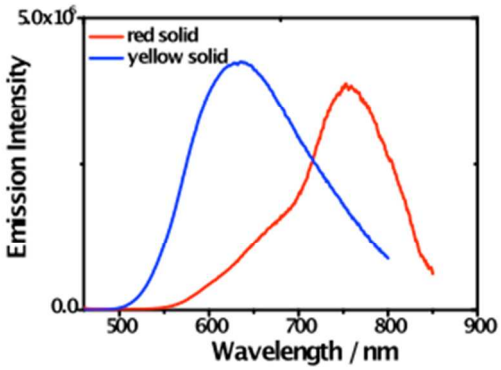

Figure 8. Emission spectra of **1** in the solid state before (blue) and after (red) exposure to the vapor of acetonitrile.

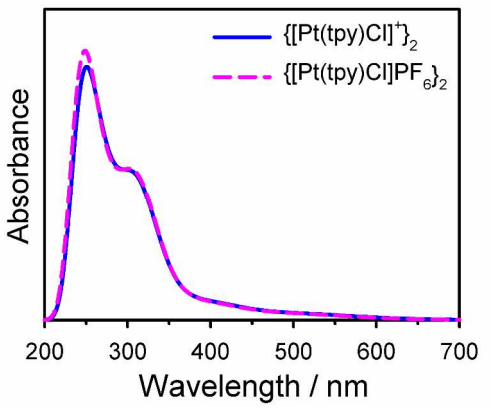

Figure 9. Calculated UV-vis spectra of the dimers of $[Pt(tpy)Cl]^+$ with or without PF_6^- counterions in acetonitrile.

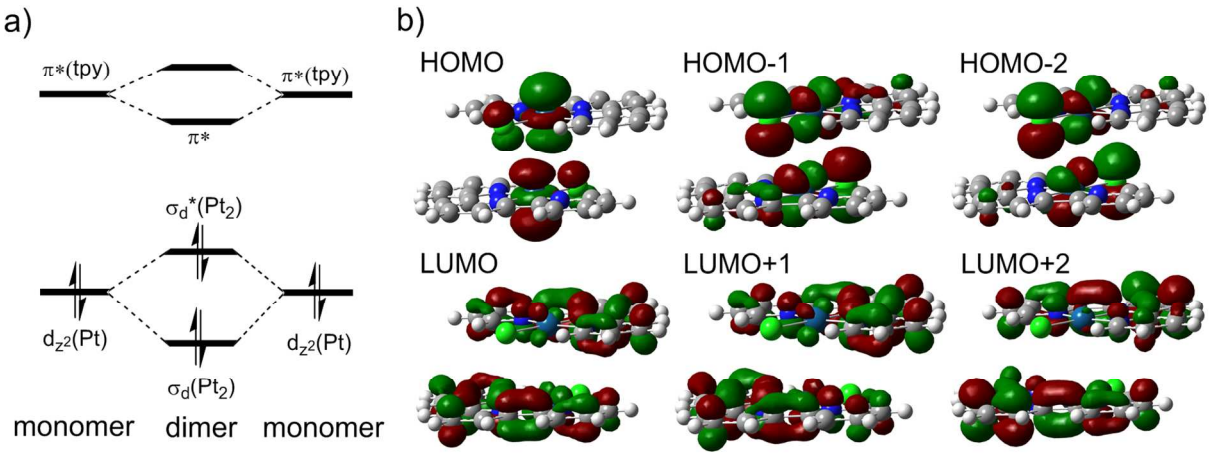

Figure 10. a) Simplified MO energy diagram for $\{[Pt(tpy)Cl]^{+}\}_2$. b) Selected MOs for $\{[Pt(tpy)Cl]^{+}\}_2$.

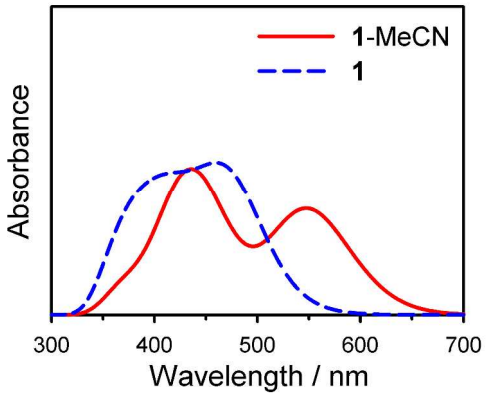

Figure 11. Calculated UV-vis spectra of **1**-MeCN and **1** using trimeric models.

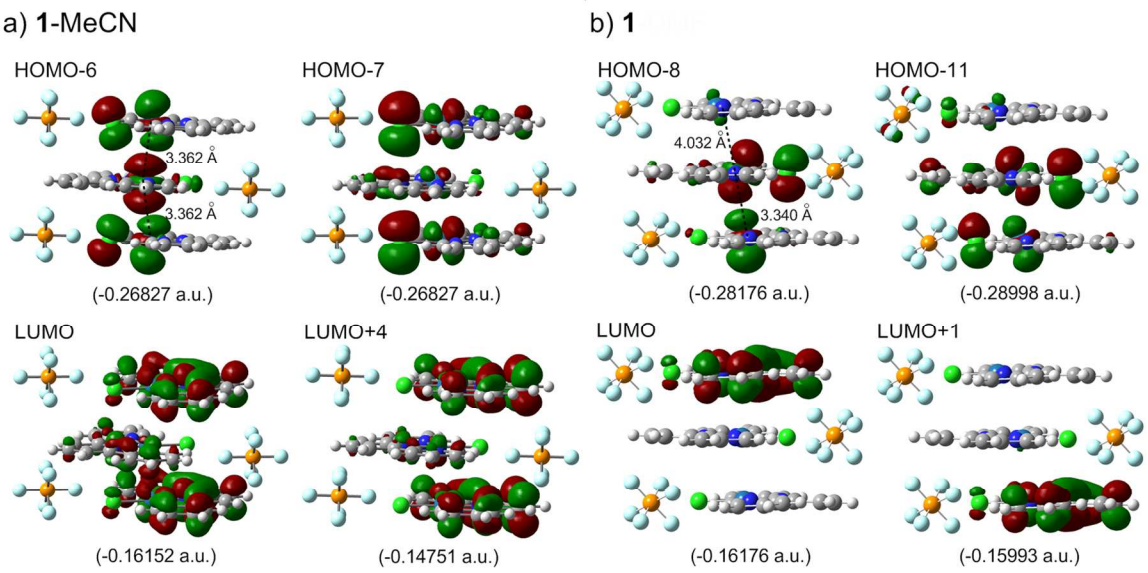

Figure 12. Selected molecular orbitals for the trimeric forms of a) **1**-MeCN and b) **1**. The orbital energies are given in parentheses.

Table 1. Crystallographic Data for **1**-MeCN

complex	**1**-MeCN
molecular formula	$C_{17}H_{14}ClF_6N_4PPt$
formula weight	649.83
temperature (K)	153(2)
radiation (λ, Å)	0.71073
crystal system	Orthorhombic
space group	*Pnma* (# 62)
a (Å)	27.144(5)
b (Å)	6.5905(13)
c (Å)	10.766(2)
α (°)	
β (°)	
γ (°)	
Volume (Å^3)	1926.0(7)
Z	4
ρ_{calcd} (g cm^{-3})	2.241
μ (mm^{-1})	7.576
crystal size (mm^3)	0.46 × 0.08 × 0.07
Theta range	2.94 to 31.50°
Completeness	99.6%
GOF	1.064
R1 (F_o)[a]	0.0434
wR2 (F_o^2)[b]	0.0978

[a] $R_1 = \Sigma||F_o| - |F_c|| / |F_o|$. [b] $wR_2 = \{\Sigma[w(F_o^2 - F_c^2)^2] / \Sigma[w(F_o^2)^2]\}^{0.5}$.

Table 2. Calculated absorption wavelength (nm), corresponding oscillator strength (*f*) and the orbitals involved in the singlet excited-states transitions of various oligomeric structures of **1**. Only excited states with $f > 0.01$ in the visible light range are listed.

Model	nm	*f*	Assignment; H = HOMO, L = LUMO
$\{[Pt(tpy)Cl]^{+}\}_2$	515.1	0.0259	H → L (97%)
(dimeric form of **1**-MeCN)	411.0	0.0507	H-2 → L (79%); H-1 → L+1 (15%)
$\{[Pt(tpy)Cl](PF_6)\}_2$	510.9	0.0253	H → L (97%)
(dimeric form of **1**-MeCN)	409.3	0.0473	H-2 → L (84%); H-1 → L+1 (10%)
$\{[Pt(tpy)Cl](PF_6)\}_3$	549.9	0.0454	H-6 → L (91%)
	463.0	0.0149	H-7 → L (74%); H-9 → L (7%); H-8 → L+1 (6%)
(trimeric form of **1**-MeCN)	438.8	0.0241	H-11 → L (71%); H-8 → L+1 (10%); H-7 → L+2 (9%)
	416.8	0.0205	H-7 → L+4 (66%); H-8 → L+3 (29%)
$\{[Pt(tpy)Cl](PF_6)\}_3$	479.6	0.0103	H-7 → L (52%); H-9 → L (29%); H-6 → L (14%)
	473.8	0.0177	H-8 → L+1 (47%); H-6 → L+1 (34%)
(trimeric form of **1**)	424.3	0.0113	H-11 → L+1 (58%); H-7 → L+1 (14%); H-6 → L+3 (8%)

Table of Contents

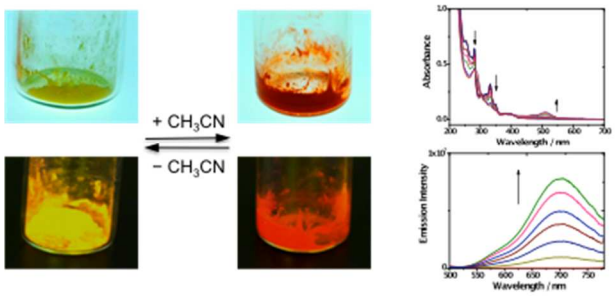

The simplest platinum(II) terpyridyl complex [Pt(tpy)Cl](PF$_6$) shows reversible response in color and emission to acetonitrile, which makes it a potentially useful sensor for this volatile organic compound. A combination of spectroscopic methods, crystallographic analyses, and theoretical studies provide a rationale to understand the nature of this Pt(II)-tpy system and its structural and electronic response to acetonitrile.